RSC Advances

ROYAL SOCIETY OF CHEMISTRY

www.rsc.org/advances

Nano and micro-TiO_2 for the photodegradation of ethanol: experimental data and kinetic modelling

Claudia L. Bianchi[a,1], Carlo Pirola[a,1], Federico Galli[a,1], Marta Stucchi[a,1,*], Sara Morandi[b,1], Giuseppina Cerrato[b,1], Valentino Capucci[c];

[a]Dip. Chimica, Università degli Studi di Milano, via C. Golgi 19, 20133 Milan, Italy; [b]Università di Torino & NIS Inter-departmental Centre, Torino, Italy; [c]GranitiFiandre SpA, Castellarano (MO), Italy; [1]Consorzio INSTM, Firenze, Italy.

[*]marta.stucchi@unimi.it

TABLE OF CONTENTS

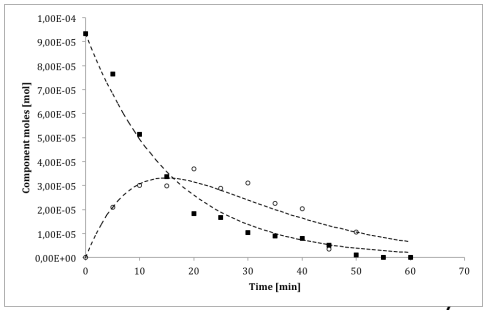

In this work we show the possibility to use pigmentary TiO_2-powders as photocatalysts and we develop a kinetic model able to follow the behavior of nano-TiO_2 versus micro-TiO_2 in Ethanol degradation.

ABSTRACT

Being TiO_2-photocatalysis an effective alternative to other more expensive Advanced Oxidation Processes (AOPs), the possibility to use micro-sized TiO_2 materials rather than the well-known nano-sized powders is an important goal in terms of both handling safety and cost saving.

In this work the photodegradation of ethanol used as a model VOC (Volatile Organic Compound) molecule was investigated comparing the efficiency of both commercial nano- and micro- sized TiO_2 samples. In all cases the same degradation pathway was observed, being it a consecutive first-order reaction with acetaldehyde as intermediate product and CO_2 and water as final products.

All photocatalysts were characterized by means of XRD, TEM, IR, BET and XPS analysis. A kinetic model was also developed considering the collected experimental data and a regression of both adsorption and kinetic constants was made using the MATLAB software. The optimized parameters were used for simulating the experimental data using the ode15s algorithm.

Keywords: Ethanol photodegradation, kinetic modelling, micrometric TiO_2, VOC, Ethanol

1. Introduction

Photocatalysis is a well-known process in which a chemical reaction occurs when a semiconductor is hit by a radiation complies with its band gap. In particular, when the semiconductor is irradiated by a light source with an appropriate wavelength, some of its electrons are transferred from the valence band to the conduction band, so creating electron-hole pairs that are able of causing reduction and oxidation reactions [1].

TiO_2 is an excellent photocatalyst used for degrading organic compounds, which are oxidized according to the mechanism aforementioned. In particular, UV irradiation induces the formation of electron-hole pairs, whose charge carriers react with chemical species such as water molecule (humidity) and molecular oxygen present in the air to produce hydroxyl radicals ($^{\bullet}OH$) and superoxide radical anions ($O_2^{\bullet-}$), respectively, which contribute to the decomposition of organic molecules at the TiO_2 surface [1,2,3].

Chemical stability and also high oxidizing power of the photogenerated holes are the main characteristics that make TiO_2 the most used and investigated photocatalyst and also the key factors for the pollutant oxidation [4].

The pollution abatement is something very important nowadays, but the worldwide research needs to develop new “green” technologies in order to limit both the energy

consumption and save money, but also to take advantages from processes with no environmental drawbacks [5]. In a sense, the TiO_2-photodegradation of pollutants, in particular organic compounds, nitrogen and sulphur oxides, is an effective alternative to the much more expensive advanced oxidation processes (AOPs) [6]. Moreover, being most of the human life spent in an indoor environment, and most of the soilage of the interior of buildings coming from VOC, their degradation is a very crucial point in order to improve both air and human health quality [4,7].

In this study, two different commercial TiO_2 samples were tested in the photodegradation reaction of ethanol, chosen as model molecule, but also considering it as an important atmospheric pollutant, commonly used as industrial solvent and a fuel additive; its oxidation is of interest because it is emitted from many industrial processes such as breweries and bakeries. Ethanol emissions accounted for about 4% of the total VOCs anthropogenic emissions in the UK in 1993 [8].

Moreover, the atmospheric concentrations of this pollutant are rising as a consequence of the use of ethanol as biofuel in the automotive sector and it is well established that this fact implies an increase in the atmospheric levels of acetaldehyde, which is far more toxic and reactive in the atmosphere than ethanol [9,10]. Besides this, acetaldehyde, also present in the ethanol photodegradation pathway, is an important indoor pollutant itself, released by some building materials such as polyurethane foams, and some consumer products such as cigarettes, adhesives, coatings and inks [11]. In fact, ethanol is first oxidized to acetaldehyde and then completely degraded to carbon dioxide and water.

The possibility to use common pigmentary micro-sized TiO_2 as photocatalyst has already been proved [12], and, although a reduced crystal size ensures an higher surface

area (that is positive in terms of photocatalytic activity), it is a disadvantage in term of safety and product handling; in fact, nano-powders can be very dangerous for health, as reported in several recent papers [13,14]. A nano-material consists of one or more components, present in various forms, that possesses at least one-dimensional structure with an average diameter in the 1-100 nm range. A quick search through the literature shows that the bulk of the research articles on nanomaterials genotoxicity were published within the past 3 years, even though their cytotoxicity and carcinogenic responses, both in vitro and in vivo, were assessed previously [15]. As the development of nanotechnological applications continue to grow, it is anticipated that there will be an even greater demand for safety, health and risk assessments studies in the forthcoming years [16].

In the present paper, two micrometric commercial samples and the well-known nano-sized P25 by Evonik have been chosen with a two-fold aim: *i.e.*, not only to evaluate the semiconductor efficiency, considering the different crystallites size, but also to verify the ethanol photodegradation pathway with all the tested materials.

From a kinetic point of view, the whole process can be simplified considering a first reaction on the catalyst surface, in which the adsorbed ethanol is converted to the adsorbed acetaldehyde, followed by a second reaction, in which the adsorbed acetaldehyde is mineralized to carbon dioxide and water, following a Langmuir-Hinshelwood mechanism. The experimental data gathered were used for the regression of the characteristics kinetic parameters, assuming pseudo first order kinetic constants.

2. Experimental

Ethanol is a Fluka product at high purity grade (99.9%). Three powdered commercial TiO_2 samples were selected without further treatment before their characterization and use: (i) a nanometric sample by Evonik (P25), always used as photocatalytic reference material and (ii) two micrometric samples (1077 by Kronos and A-HR by Hunsdman), sold as pigment and chosen with the following features: pure anatase, untreated surfaces, undoped material, powdery form.

2.1 Samples characterization

Surface area of all catalysts was determined by conventional N_2 adsorption (BET) at 77 K using a Sorptometer instrument (Costech Mod. 1042).

X-ray photoelectron spectra (XPS) were taken in an M-probe apparatus (Surface Science Instruments). The source was monochromatic Al Kα radiation (1486.6 eV).

The morphology of the catalysts was inspected by means of high-resolution transmission microscopy (HR-TEM): images were recorded using a JEOL 3010-UHR instrument (acceleration potential: 300kV; LaB_6 filament).

Absorption/transmission IR spectra were obtained on a Perkin-Elmer FT-IR System 2000 spectrophotometer equipped with a Hg-Cd-Te cryo-detector, working in the 7200-580 cm^{-1} range at a resolution of 2 cm^{-1} (number of scans ~20). ~~For~~ Before the IR analysis, powdery samples were compressed in self-supporting discs (of about 10 mg cm^{-2}) and placed in a homemade quartz cell, equipped with KBr windows, connected to a conventional high-vacuum line (UHV). Spectra were recorded at room temperature (RT) on the samples in air or after prolonged outgassing at RT.

For the characterization of the light absorption features and band-gap determinations, diffuse reflectance spectra (DRS) of the powders were collected using a UV-vis

scanning spectrophotometer (PerkinElmer, Lambda 35), which was equipped with a diffuse reflectance accessory.

The XRD spectra were collected using a PW 3830/3020 X' Pert Diffractometer from PANalytical working Bragg-Brentano, using the Cu $K_{\alpha 1}$ radiation (λ = 1.5406 Å).

2.2 Photocatalytic tests

Photocatalytic degradations were conducted in a cylindrical glass reactor (diameter=200 mm, Volume=5 L). The amount of catalyst used in each test was 0.05 g and it was deposited on a glass support as a thin film: the latter is obtained preparing a suspension of isopropanol and TiO_2, and depositing it on the glass slide through a Pasteur pipette [17]. The reactor was initially charged with chromatographic air humidified at 40% RH. The starting ethanol concentration was set at 400 ppmv. Photon sources were provided by a 500 W UV lamp (Jelosil model HG 500) emitting in 315-400 nm wavelength range (UV-A) at 30 Wm^{-2} on the sample surface and each test lasted 4 h [18]. The ethanol photodegradation was monitored, using an on-stream gas chromatography (Agilent 3000 A microGC), directly connected to the reactor, that automatically measures the internal concentration of ethanol, acetaldehyde and carbon dioxide.

Photolysis tests were also performed for both pure ethanol and acetaldehyde to monitor the possible molecule degradation under UV light in the absence of photocatalyst. The same procedure was repeated using acetaldehyde. Adsorption tests were also carried out by monitoring the concentration for 4 hours for both ethanol and acetaldehyde in the dark to obtain the adsorption constants (K) separately, in order to reduce the model parameters to be estimated. This approach has been already used in literature for the

143 independent determination of adsorption and kinetic constants [19,20].

144 All the photocatalytic tests carried out on each powder have been repeated at least 5
145 times, exhibiting the same behavior for each run.

146 The regression of both the adsorption and the kinetic constants were made using
147 MATLAB software, minimizing the sum of the squared errors between the calculated
148 and the experimental data. The optimized parameters were used for simulating the
149 experimental data using a differential equation solver able to handle stiff problem, i.e.
150 the ode15s algorithm [21].

151

152 3. Results and discussion

153 3.1 Morphological characterization

154 The morphological characteristics of all the used catalysts are reported in Table 1.

155 **Table 1**
156 Main features of the selected TiO_2 samples.

Sample	Anatase/Rutile composition	BET surface area (m^2g^{-1})	Average crystallite size (nm)	XPS Ti $2p_{3/2}$ (eV)	XPS OH/O_{tot}	Band Gap (eV)
P25	80% Anatase 20% Rutile	52	26	458.4	0.14	3.21
1077	100% Anatase	11	130	458.4	0.32	3.15
A-HR	100% Anatase	12	130	458.0	0.14	3.15

157

158 XRD analysis confirms the well-known P25 phase composition, 80:20 in anatase/rutile
159 ratio, and shows that anatase is the unique polymorph for the other two samples, 1077

and A-HR. One of the most critical drawbacks of both micrometric samples is their low specific surface area; however, the presence of the bare anatase polymorph is confirmed, and this is a fundamental feature in term of the photocatalytic performance.

As for the general morphology of the various samples, low magnification TEM images have been reported in Figure 1. It is evident that P25 totally reveals its nano-sized nature (average particle size ~ 20-30 nm) if compared to both 1077 and A-HR powders (for which the average particles size is much higher, lying in the 100-180 nm range). The high-resolution images relative to all the samples (see the inset in each image reported in Figure 1) confirm the high crystallinity exhibited by the powders and the phase composition, as well.

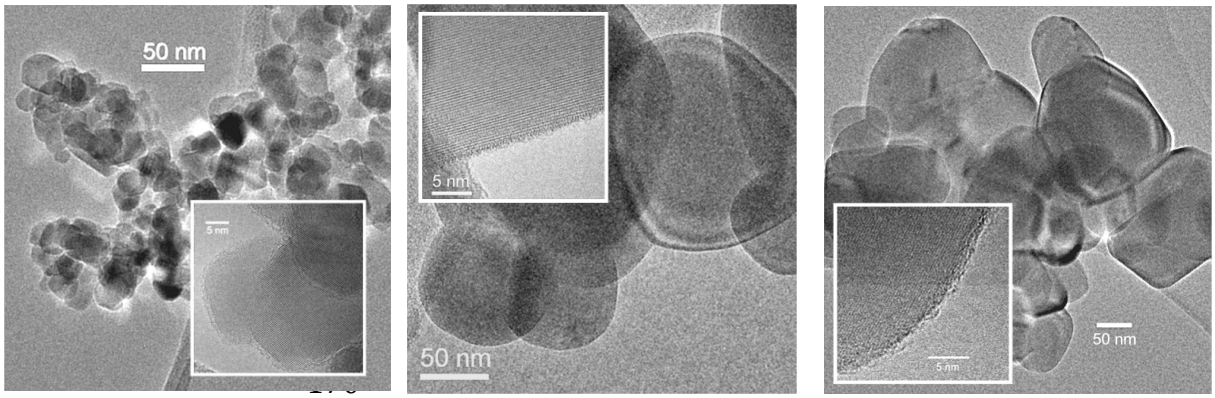

P25 Kronos A-HR

Fig. 1: TEM images of the various TiO_2 samples

BET surface area data are consistent with the above considerations: in fact, a particles size located in the nano-size range, as in case of P25, implies a much higher surface area and viceversa the opposite trend is expected for the micro-sized powders (see Table 1, column 2-3).

The surface state of the TiO_2 particles was analyzed by XPS. No significant differences can be appreciated in the Ti 2p region concerning the binding energies (BE). The peak Ti $2p_{3/2}$ is always regular and the BE (see Table 1, column 4) compares well with the data for Ti(IV) reported in the literature for TiO_2 materials [22]. The analysis of the oxygen peaks reveals the presence of more than one component, which can be attributed to lattice oxygen in TiO_2 (529.9 eV) and to surface OH species (> 531.5 eV), respectively [19].

The hydrophilicity/hydrophobicity character of photocatalysts surface plays a crucial role in determining the ethanol adsorption and thus the final photocatalytic activity, at least in the degradation of pollutants [23]. The sixth column of Table 1 reports the OH/O_{tot} surface ratio, which refers to a quantitative measure of the hydrophilicity/hydrophobicity of the TiO_2 surface, estimated using the XPS (Fig. 2) [23,24]. On one hand, P25 material exhibits the lowest OH/O_{tot} ratio, and its better activity is surely related to its higher surface area, that ensures a bigger amount of surface OH groups as evidenced by FTIR spectra (see Fig. 2, section B) in the region of absorption bands related to H-bonded and free hydroxyls (these last evidenced by grey box). In particular P25, differently from both Kronos and AH-R samples, exhibits a larger amount with high heterogeneity of free hydroxyls, the most important species for the degradation reaction [18]. On the other hand, different values of the OH/O_{tot} ratio result in a very similar activity in case of both Kronos 1077 and AH-R powders: this is related to the fact that the XPS analysis gives a result which refers to the entire number of OH groups. FTIR spectra (Fig. 2, section B) put in evidence a quite larger amount of H-bonded OH groups for Kronos 1077, but very similar features of free OH for both the samples.

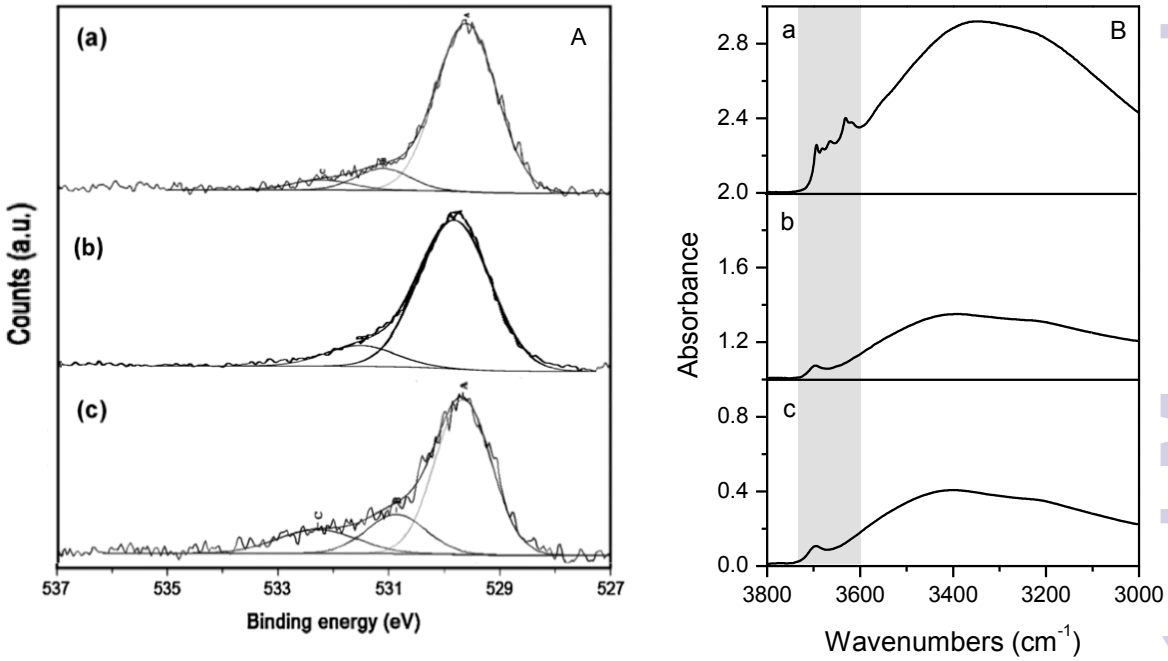

Fig. 2: O_{1s} XPS Spectra (A) and FTIR spectra (B) recorded at RT in air for (a) P25, (b) A-HR, (c) 1077.

3.2 Kinetic Parameters regression

The degradation reaction is followed considering this pathway [14]:

$$\begin{cases} (1)\ CH_3CH_2OH_{ads} \xrightarrow{k_1} CH_3COH_{ads} \\ (2)\ CH_3COH_{ads} \xrightarrow{k_2} 2\,CO_2 + H_2O \end{cases}$$

Photocatalyzed reactions in which a gas phase reactant is involved are usually interpreted using the Langmuir-Hinshelwood mechanism [25], where only the reactant molecules previously adsorbed on the catalytic surface take part to the reaction. This kinetic interpretation is well-known for photocatalyzed reactions, as reported in some papers herein [26, 27].

For what concern the regression of the kinetic parameters in the present paper, two consecutive first order reactions were considered, as showed in the scheme reported in the introduction section. The differential equation system that characterizes the system is here reported:

$$\begin{cases} \frac{dn_e}{dt} = -k_1 * \frac{K_e * n_e}{1 + K_e * n_e + K_a * n_a} \\ \frac{dn_a}{dt} = +\frac{k_1 * K_e * n_e - k_2 * K_a * n_a}{1 + K_e * n_e + K_a * n_a} \\ \frac{dn_{CO_2}}{dt} = +2 * k_2 * \frac{K_a * n_a}{1 + K_e * n_e + K_a * n_a} \end{cases} \quad (1)$$

Ke and Ka (mol^{-1}) are the adsorption constant for ethanol (e) and acetaldehyde (a) and k_1 and k_2 ($mol\ min^{-1}$) the first order kinetic constant. As can be observed the adsorption of CO_2 was not considered.

The adsorption constants (K_i) were obtained considering a reversible adsorption for both ethanol and acetaldehyde. The differential equation used for this regression is:

$$\frac{dn_i}{dt} = -k_{ads,i} * n_i + k_{des,i} * (n_{0,i} - n_i)$$

In which is either ethanol or acetaldehyde, $n_{0,i}$ the moles of the component charged in the reactor and n_i the mole of the component at a certain time. The adsorption constant is then calculated by dividing k_{ads} by k_{des} after the regression.

3.3 Photolysis and adsorption tests

In order to determine the real role of the photocatalytic process, both photolysis and simple ethanol absorption were investigated.

The photolysis contribution is negligible, and it can be concluded that both ethanol and its oxidized intermediate product, i.e. acetaldehyde, are not sensible to the bare UV light, and their concentrations remain stable for the entire test.

Different is the role of the absorption: reported in Figure 4 a (P25) and b (Kronos 1077). (AH-R sample gave very similar results to the 1077 adsorption and are not reported for the sake of clarity).

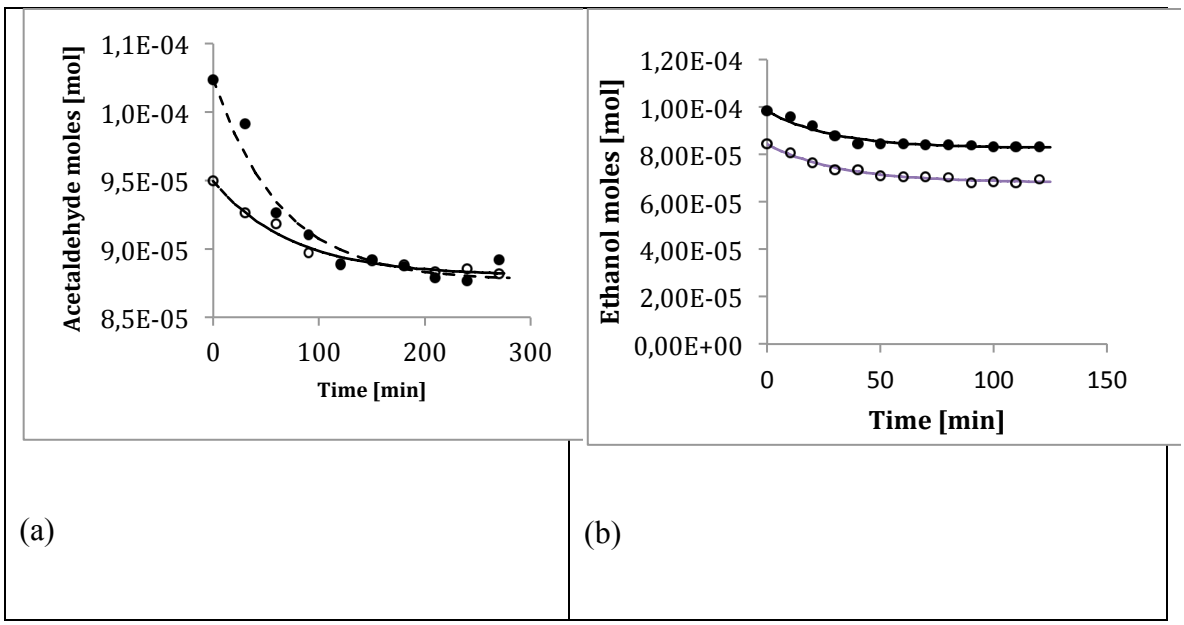

Fig. 3: Adsorption runs of a) acetaldehyde and b) ethanol on P25 (○) and 1077 (●). Dotted lines are the calculated curved using the regressed adsorption constants.

The optimized adsorption constants calculated from these experimental data are reported in Table 2:

	Adsorption constant K [mol^{-1}]		
Component	P25	1077	A-HR
Ethanol	0.2373	0.1891	0.1884
Acetaldehyde	0.0786	0.1680	0.1809

Table 2: adsorption constants regressed from experimental data

The results indicate that P25 possesses a higher adsorption constant for ethanol if compared to that exhibited by both micrometric samples. On the contrary, acetaldehyde results show an opposite trend and the adsorption of these species seems to have no relation with the OH/O surface ratio of the catalyst.

In Figures 5-7 the experimental data obtained in the photocatalytic runs performed using the different catalysts have been reported, together with the calculated trend using the optimized kinetic parameters:

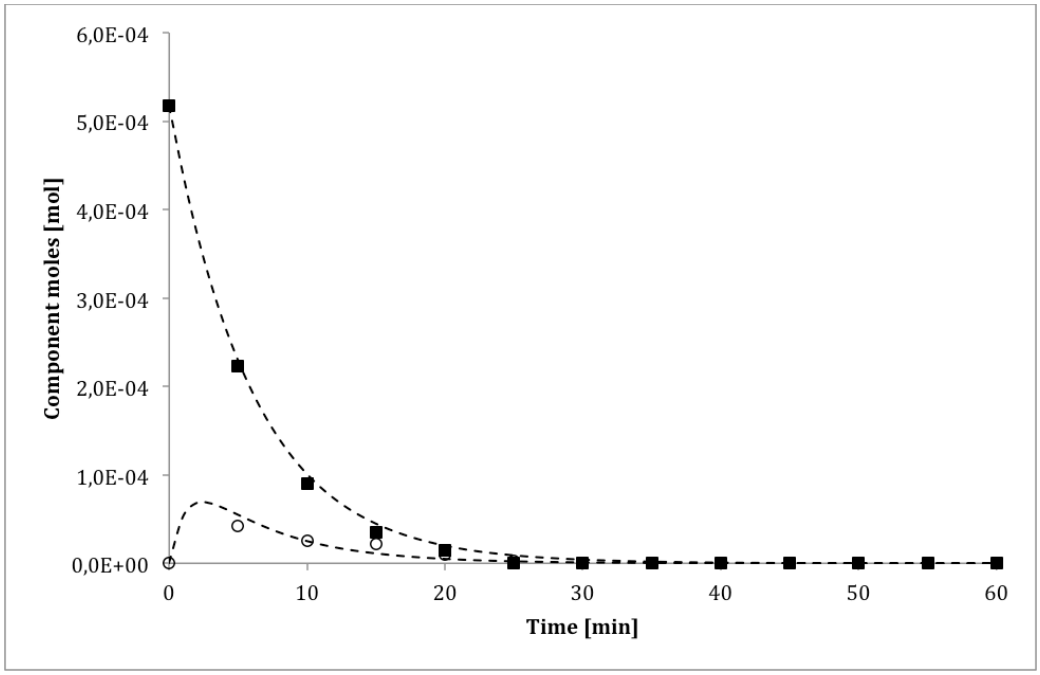

Fig. 4: Experimental ethanol photodegradation tests performed using P25 catalyst. Empty points represents acetaldehyde. Dotted lines are the simulated trends obtained using the regressed kinetic constant.

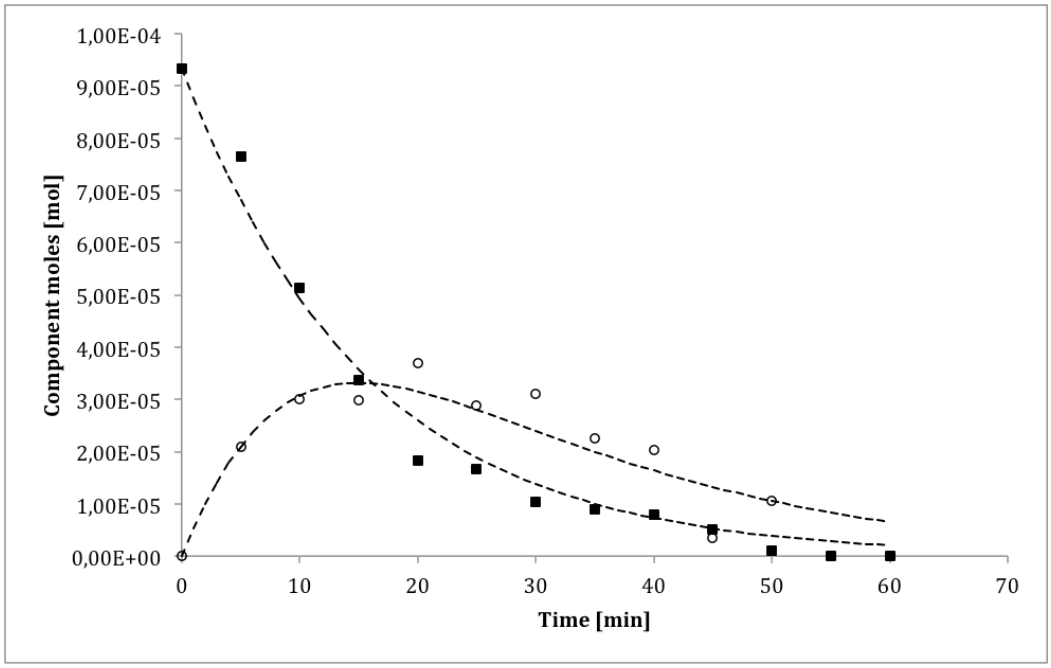

Fig. 5: Experimental ethanol photodegradation tests performed using 1077 catalyst. Empty points represent acetaldehyde. Dotted lines are the simulated trends obtained using the regressed kinetic constant.

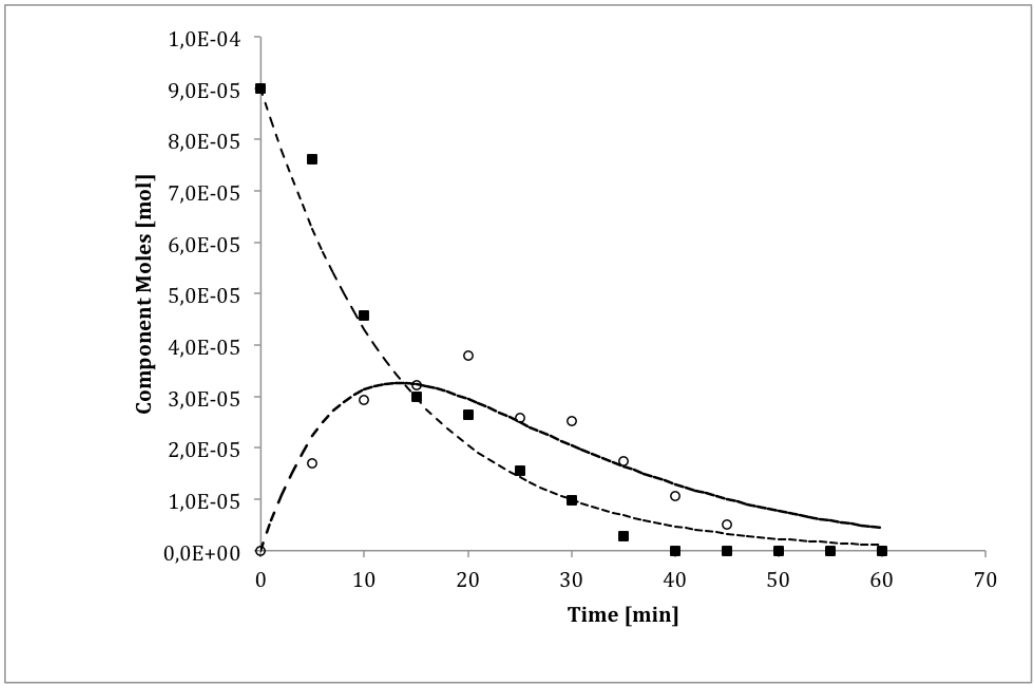

Fig. 6: Experimental ethanol photodegradation tests performed using A-HR catalyst. Empty points represent acetaldehyde. Dotted lines are the simulated trends obtained using the regressed kinetic constant.

The regressed kinetic parameters are reported in Table 3:

Table 3: regressed kinetic constant for all the photocatalysts

Sample	k_1 [mol min^{-1}]	k_2 [mol min^{-1}]	SSE
P25	0.68	10.41	$3.91*10^{-9}$
1077	0.34	0.42	$1.69*10^{-9}$
AHR	0.39	0.42	$6.88*10^{-10}$

The simulated results, obtained with the optimized kinetic parameters, exhibit a good fit for the test performed using both P25 and the micrometric samples, confirmed also by the low value of the sum of the squared errors (SSE). It is possible to observe the great difference between nanometric (P25) and micrometric (AHR and 1077) samples. In fact, the numerical values of both kinetic constants are larger for P25, in agreement with its superior catalytic performance. Moreover, for this sample the k2 constant is one order of magnitude larger than the corresponding k1 constant; this means that, using nano-sized catalysts, the degradation of acetaldehyde is very fast with respect to the conversion of ethanol. The situation is completely different when the reactions are catalysed by micrometric samples. In fact, using these catalysts, both the numerical values of k1 and k2 kinetic constants and the numerical value of the constants between 1077 and AHR sample are very similar. The analysis of the kinetic elaboration gives us important information about the rate of reaction using either nanometric or micrometric samples. The rate of VOC degradation is in general increased if catalysed by nanometric sample with respect the micrometric ones, being this phenomenon particularly important for some light compounds (i.e., acetaldehyde). Nevertheless, the catalytic properties of micrometric samples are confirmed from both the direct experimental conversion and this kinetic interpretation. In particular, considering the

degradation of ethanol, the rate of its conversion is not so different for either nanometric or micrometric samples.

FTIR data obtained for TiO_2 powders, either before and after the photodegradation processes, indicate that ethanol leaves some residues (traces) onto the surface of the supports, independently of their micro- or nanosized nature: see for instance Figure 7, in which we reported the results relative to the nanometric P25 powder (top section of the Figure) and to one of the two micrometric materials, namely Kronos 1077 (bottom section of the Figure), as the A-HR powder exhibited a trend (almost) coincident to that of Kronos 1077.

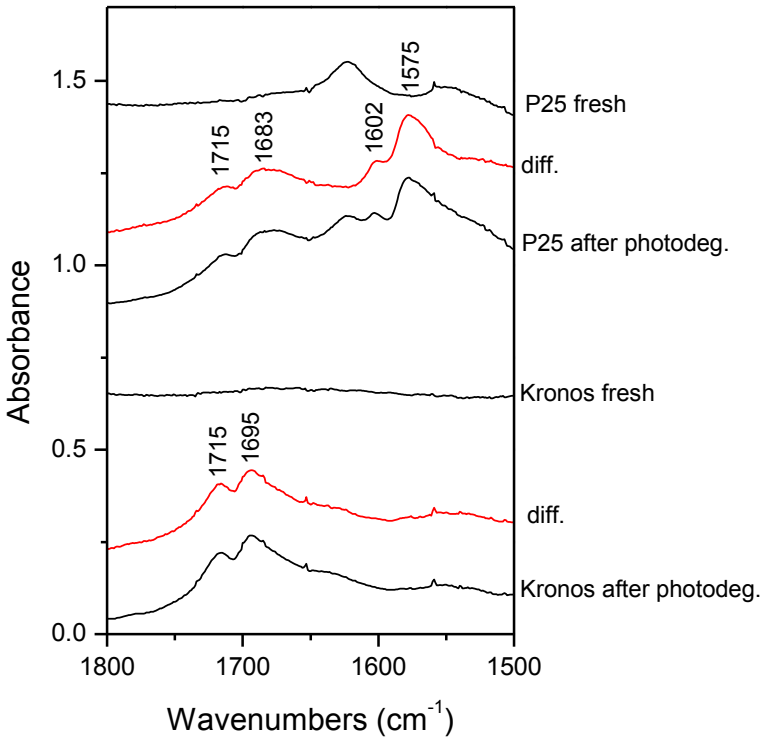

Fig. 7: Absorbance FTIR spectra relative to fresh and used in ethanol degradation reaction P25 (top spectra) and 1077 (bottom) TiO_2 samples. The differences between spectra of the samples after and before ethanol degradation are reported in red.

In fact, if we refer to the spectral range (1800-1500 cm^{-1}) in which the $\nu_{C=O}$ mode(s) typical of the possible degradation products of ethanol (ketone/aldehyde) are normally located [28], two net components are evident at ~ 1715 and ~ 1695-83 cm^{-1}. This confirms that an effective degradation has occurred, but a few (really only traces) of the degraded products are still present at the surface of the TiO_2 powders. Moreover, for the P25 material other spectral components, located at 1602 and 1575 cm^{-1}, reveal the presence of short chain carboxylated species (namely, acetate/formate species) chemisorbed to the TiO_2 surface. This puts into evidence the formation of acetic acid as an intermediate in acetaldehyde degradation at least in the case of the nano-sized photocatalyst here considered.

This is also in agreement with the calculated kinetic parameters reported in Table 2. In fact, the P25 material, due to its intrinsic nanometric nature, confirms to have the best performances as photocatalyst, particularly for the degradation of acetaldehyde, being the (k_2) kinetic constant an order of magnitude larger, if compared to that of micrometric samples.

However, considering the bare ethanol degradation, the micrometric samples are able to oxidize it almost completely and thus can be employed for its degradation, being them far less dangerous for human health.

4. Conclusions

The photodegradation of ethanol, as a model for VOCs, was performed using a commercial nanometric sample and two different micrometric powders. Well as having presented this model, the possibility to exploit the photocatalytic potential of the

pigmentary TiO_2 is proved, giving a contribution to the already useful photocatalytic processes. The micrometric TiO_2, less dangerous and much less expensive with respect to the nanometric P25, is active as photocatalysts, being able to degrade VOCs into CO_2, also if with rate of reaction, and then kinetic constants, lower respect the P25. The good fitting between experimental and simulated results confirm the assumption of a consecutive first order reaction mechanism, degradation pathway that is not influenced by the TiO_2 crystallites dimension.

Acknowledgements

This research was supported by LIFE+ Environment Policy and Governance project LIFE13 ENV/IT/000140.

References

[1] K. Nakata, T. Ochiai, T. Murakami, A. Fujishima, Electrochim. Acta 84 (2012) 103–111.

[2] A. Fujishima, X. Zhang, D. A. Tryk, Surf. Sci. Rep. 63 (2008) 515–582.

[3] K. Nakata, A. Fujishima, J. Photochem. Photobiol. C 13 (2012) 169–189.

[4] A. Fujishima, T.N. Rao, D.A. Tryk, J. Photochem. Photobiol. C 1 (2000) 1–21.

[5] J. Lyu, L. Zhu, C. Burda, Catal. Today 225 (2014) 24–33.

[6] M. Sievers, Advanced Oxidation Processes.

[7] Y. Xu, Y. Zhang, Atmos. Environ. 38 (2004) 113–119.

[8] R.G. Derwent, M.E. Jenkin, S.M. Saunders, Atmos. Environ. 30 (1996) 181–199.

[9] E.M. Martins, S.M. Correa, G. Arbilla, Brazil Atmos. Environ. 37 (2003) 23–29.

[10] M. Colón, J.D. Pleil, T.A. Hartlage, M.L. Guardani, M.H. Martins, Brazil Atmos. Environ. 35 (2001) 4017–4403.

[11] D. Meroni, S. Ardizzone, G. Cappelletti, C. Oliva, M. Ceotto, D. Poelman, H. Poelman, Catal. Today 161 (2011) 169–174.

[12] C. L. Bianchi, C. Pirola, F. Galli, G. Cerrato, S.Morandi, V. Capucci, Chem. Eng. J. 261 (2014) 76-82.

[13] S. Bakand, A. Hayes, F. Dechsakulthorn, Inhal. Toxicol. 24 (2012) 35-125.

[14] M.A. Albrecht, C.W. Evans, C.L. Raston, Green Chem 8 (2006) 417–32.

[15] B. Trouiller, R. Reliene, A. Westbrook, P. Solaimani, R.H. Schiestl, Cancer Res. 69 (2009) 8784–8789.

[16] N.G. Cheng-Teng, J.J. Li, B.H. Bay, L.Y. Lanry Yung, J. Nucleic Acids 2010 (2010), Article ID 947859, http://dx.doi.org/10.4061/2010/947859.

[17] C.L.Bianchi, C.Pirola, E.Selli, S.Biella, J. Hazard Mater. 211–212 (2012) 203–207.

[18] C.L. Bianchi, S. Gatto, C. Pirola, A. Naldoni, A. Di Michele, G. Cerrato, V. Crocellà, V. Capucci, Appl. Cat. B: Environmental 146 (2014) 123-130.

[19] T. Popken, L. Gotze, J. Gmehling, Ind. Eng. Chem. Res. 39 (2000) 2601–2611.

[20] W. Song, G. Venimadhavan, J.M. Manning, M.F. Malone, M.F. Doherty, Ind. Eng. Chem. Res. 37 (1998) 1917.

[21] L.F. Shampine, M.W. Reichelt, SIAM J. Sci. Comput. 18 (1997) 1-22.

[22] G. Cappelletti, C.L. Bianchi, S. Ardizzone, Appl. Surf. Sci. 253 (2006) 519–524.

[23] S. Ardizzone, C.L. Bianchi, G. Cappelletti, A. Naldoni, C. Pirola, Env. Sci. Technol. 42 (2008) 6671–6676.

[24] S. Ardizzone, C.L. Bianchi, G. Cappelletti, S. Gialanella, C. Pirola, V. Ragaini, J. Phys. Chem. C 111 (2007) 13222–13231.

[25] C. S. Turchi, D. F. Ollis, J. Catal. 122 (1990) 178-192.

[26] M.L. Sauer, D.F. Ollis, J. Catal. 158 (1996) 570–582

[27] I.K. Konstantinou, T.A. Albanis, Appl. Cat. B Environ. 49 (2004) 1–14.

[27] L.H. Little, Infrared Spectra of Adsorbed Species, Academic Press, London, 1966.

Tables and figure legends

Table 1 Main features of the selected TiO_2 samples.

Table 2: adsorption constants regressed from experimental data

Table 3: regressed kinetic constant for all the photocatalysts

Figure 1: TEM images of the various TiO_2 samples

Figure 2: O_{1s} XPS Spectra (A) and FTIR spectra (B) recorded at RT in air for (a) P25, (b) A-HR, (c) 1077.

Figure 3: Adsorption runs of a) acetaldehyde and b) ethanol on P25 (○) and 1077 (●). Dotted lines are the calculated curved using the regressed adsorption constants.

Figure 4: Experimental ethanol photodegradation tests performed using P25 catalyst. Empty points represents acetaldehyde. Dotted lines are the simulated trends obtained using the regressed kinetic constant.

Figure 5: Experimental ethanol photodegradation tests performed using 1077 catalyst. Empty points represent acetaldehyde. Dotted lines are the simulated trends obtained using the regressed kinetic constant.

Figure 6: Experimental ethanol photodegradation tests performed using A-HR catalyst. Empty points represent acetaldehyde. Dotted lines are the simulated trends obtained using the regressed kinetic constant.

Figure 7: Absorbance FTIR spectra relative to fresh and used in ethanol degradation reaction P25 (top spectra) and 1077 (bottom) TiO_2 samples. The differences between spectra of the samples after and before ethanol degradation are reported in red.